Modeling myosin Va liposome transport through actin filament networks reveals a percolation threshold that modulates transport properties

S. Walcott[a,*] and D. M. Warshaw[b]
[a]Department of Mathematical Sciences, Worcester Polytechnic Institute, Worcester, MA 01609; [b]Molecular Physiology and Biophysics, University of Vermont, Health Science Research Facility, Burlington, VT 05405

ABSTRACT **Myosin Va (myoVa) motors transport membrane-bound cargo through three-dimensional, intracellular actin filament networks. We developed a coarse-grained, in silico model to predict how actin filament density (3-800 filaments) within a randomly oriented actin network affects fluid-like liposome (350 nm vs. 1750 nm) transport by myoVa motors. Five thousand simulated liposomes transported within each network adopted one of three states: transport, tug-of-war, or diffusion. Diffusion due to liposome detachment from actin rarely occurred given at least 10 motors on the liposome surface. However, with increased actin density, liposomes transitioned from primarily directed transport on single actin filaments to an apparent random walk, resulting from a mixture of transport and tug-of-wars as the probability of encountering additional actin filaments increased. This phase transition arises from a percolation phase transition at a critical number of accessible actin filaments, N_c. N_c is a geometric property of the actin network that depends only on the position and polarity of the actin filaments, transport distance, and the liposome diameter, as evidenced by a fivefold increase in liposome diameter resulting in a fivefold decrease in N_c. Thus in cells, actin network density and cargo size may be regulated to match cargo delivery to the cell's physiological demands.**

Monitoring Editor
Alex Mogilner
New York University

Received: Aug 11, 2021
Revised: Dec 13, 2021
Accepted: Dec 14, 2021

INTRODUCTION

In eukaryotic cells, intracellular cargo transport, such as insulin granules that are destined for secretion at the cell membrane, is shared by molecular motors that travel along the microtubule and actin cytoskeletal highways (Ross *et al.*, 2008). Beginning at the Golgi where secretory vesicles are formed, kinesin motors provide long-range transport along microtubules oriented toward the cell membrane. Final short-range transport and delivery to the cell membrane relies on vesicle hand off to myosin Va (myoVa) motors that maneuver their cargo through the dense, randomly oriented cortical actin filament network (Tabb *et al.*, 1998; Wagner *et al.* 2011; Hammer and Sellers, 2012; Baladanyan and Arnold, 2014). However, the precise role of myoVa in cells is still debated, whether it is a short- or long-range transporter for cargo delivery to a targeted location or whether myoVa tethers cargo to the actin network in close proximity to the cell membrane (Gross *et al.*, 2002; Desnos *et al.*, 2007; Schuh, 2011; Hammer and Sellers, 2012; Evans *et al.*, 2014). Are these putative myoVa roles compatible with an apparently random network of actin filaments with which the motors are engaged or does the structure of the actin filament network itself dictate which functional role myoVa motors adopt? The importance of these questions is underscored by genetic mutations in myoVa that lead to mislocalized cargo in cells (Provance *et al.*, 1996) and neurological defects in humans (Pastural *et al.*, 1997; Takagishi and Murata, 2006).

To define the challenges that myoVa motors face when navigating cargo through the cell's three-dimensional (3D) actin filament network, investigators have built complexity in vitro within model transport systems, ranging from single myoVa transport, as the motor steps toward the plus-end of a single actin filament, to more complex liposome transport by teams of myoVa motors through 3D actin filament networks (Veigel *et al.*, 2002; Forkey *et al.*, 2003;

This article was published online ahead of print in MBoC in Press (http://www.molbiolcell.org/cgi/doi/10.1091/mbc.E21-08-0389) on December 22, 2021.

*Address correspondence to: S. Walcott (swalcott@wpi.edu).

Abbreviations used: myoVa, myosin Va; SM, supplementary material; 3D, three dimensional.

Yildiz *et al.*, 2003; Warshaw *et al.*, 2005; Ali *et al.*, 2007; Nelson *et al.*, 2014; Lombardo *et al.*, 2017, 2019). Understanding the molecular bases for transport outcomes in these in vitro experiments has relied on mechanistic mathematical modeling. These models incorporate numerous aspects of myoVa molecular structure and function but most importantly the force-dependent slowing of myoVa's stepping rate when the motor experiences a hindering force applied externally to the cargo or due to a "tug-of-war" between motors on the same cargo that interact simultaneously with separate actin filaments (Lan and Sun, 2005; Vilfan, 2005; Nelson *et al*, 2014). In silico modeling of this latter scenario was critical to our previously interpreting the trajectories of liposomes transported by a myoVa team through 3D actin networks (Lombardo *et al.*, 2017, 2019), providing insight into how the density and orientation of the local actin network surrounding the liposome dictated the motors' short-range (~1 μm, 1–10 s) modes of transport motion (i.e., directed, diffusive-like, or stationary). However, these previous in vitro studies were limited experimentally since exploring the vast experimental parameter space, such as the effects of cargo diameter and actin network density, was both technically and analytically demanding. Thus there remains a critical gap between these in vitro experiments and myoVa's function in cells, where cargo transport to a destination can occur over longer spatial and temporal scales (~tens of μm, minutes).

Mathematical models can help bridge the gap between the molecular and the larger intracellular scales. Models keep track of a multitude of molecular-scale processes that occur simultaneously and impact each other, often leading to emergent properties (e.g., phase transitions). For example, phase transitions in the macroscopic mechanical properties of cross-linked actin networks in the presence of myosin-II filaments, i.e., whether the system flows like a fluid (Goff *et al.*, 2001, Liverpool *et al.*, 2001; Humphrey *et al.*, 2002), remains solid like a gel (Mizuno *et al.*, 2007; Koenderink *et al.*, 2009) or contracts into one (Bendix *et al.*, 2008) or more (Soares e Silva *et al.*, 2011; Murrell and Gardel, 2012) dense clusters, can be understood through mathematical modeling (Sheinman *et al.*, 2012a,b; Alvarado *et al.*, 2017). Here we use in silico modeling to investigate how myoVa-based cargo transport through a random 3D actin filament network over spatial and temporal scales observed in cells (~tens of μm, minutes) is affected by actin filament density within the network and by cargo diameter. We find that such long-range myoVa-based transport shows a cargo size-dependent phase transition as actin density is varied. Specifically, at low actin density, transport is rapid and unidirectional. In contrast, above a critical actin density that scales linearly with travel distance and inversely with cargo diameter, transport is interrupted by pauses and loss of directionality as motor teams undergo tug-of-wars and switch filaments, respectively. Cells may take advantage of this phase transition to switch roles between myoVa acting as a long range transporter or tether.

RESULTS

Model of long-range liposome transport

In this study we used in silico modeling to define how long-range vesicular transport by myoVa motors through an actin filament network would be impacted by changes in actin filament density and cargo diameter. The foundation for this work was our previously developed and experimentally validated, in silico mechanistic model for the transport of 350 nm (radius r_L = 175 nm) fluid membrane liposomes by teams of 10 myoVa motors through actin filament networks (Lombardo *et al.*, 2017, 2019). However, this model probed short-range myoVa transport (~1 μm, 1–10 s) within a limited actin filament network (i.e., several actin filaments) rather than transport over spatial and temporal scales observed in cells (~tens of μm, minutes). Therefore using the same liposome-motor complex, we modeled transport through a series of complex actin filament networks confined within a 20-μm diameter sphere (Figure 1). These actin networks consisted of a variable number of randomly placed filaments covering roughly three orders of magnitude (i.e., 3–800 filaments; see Supplemental Movies S1–S6). Since all networks were confined to the same diameter sphere, the number of actin filaments within the sphere can be used interchangeably with actin density. For each actin filament network, we simulated 5000 liposome trajectories that all started with the liposome bound to an actin filament at the network center (Figure 1A, t = 0 s). A trajectory concluded when either the liposome reached the boundary of the sphere or 100 s elapsed. In total, we simulated 1,040,000 liposome trajectories for the various model conditions. However, given our experimental parameter space, using our previous model algorithms was too computationally expensive. Therefore we implemented a coarse-grained model, described below, that allowed us to more efficiently simulate myoVa-based liposome transport over larger spatial and temporal scales.

In this coarse-grained model (see *Materials and Methods* and Supplemental Material [SM] for details), the liposome is in one of three states at any point in time (Figure 1B), undergoing 1) transport, where the liposome-motor complex is engaged with and traveling along a single actin filament; 2) tug-of-war, where motors on the same liposome interact simultaneously with separate actin filaments; or 3) diffusion, where the liposome freely diffuses with an assumed diffusion constant for a 350-nm sphere in water at 25°C (D = 1.3 μm^2/s). A liposome in the transport state travels toward the actin filament plus-end along a spiral path dictated by the actin filament helix (Ali *et al.*, 2002). Once the liposome encounters a second actin filament within reach of the motors on its surface, it may transition into the tug-of-war state. When in a tug-of-war, the liposome is stationary until the tug-of-war is resolved when either 1) motors engaged with one actin filament overcome the force generated by motors engaged with the other actin filament, thus returning the liposome to the transport state on the filament associated with the winning team of motors; or 2) all motors detach from their engaged actin filaments and the liposome transitions to the diffusion state. When in the diffusion state, the liposome can only transition to the transport state after it collides with an actin filament. Rate constants governing the transitions between states depend on the proximity of actin filaments to the liposome, while the tug-of-war duration depends on the position and polarity of the actin filaments with which the motors are engaged. The rate constants for liposome state transitions were determined by fitting this coarse-grained model to thousands of simulations of our previous, more detailed model (Lombardo *et al.*, 2017, 2019) (see SM for the fits). Once the coarse-grained model's predictive capacity was verified against the short-range predictive capacity of our previous model, long-range liposome trajectories in the various actin network models were simulated with a Monte Carlo method (Figure 1A; see SM for more algorithm details). Steric interactions between the liposome and the actin network are not included in this model, so we ensured that all actin networks had pore sizes larger than the liposome diameter (see SM).

Liposome transport simulations at varying actin network density

Simulated liposome trajectories at low actin density (3–50 filaments; Supplemental Movies S1–S4) demonstrate that most liposomes move along individual actin filaments in the transport state (blue liposome in the supplemental movies and Figures 1 and 2B) and

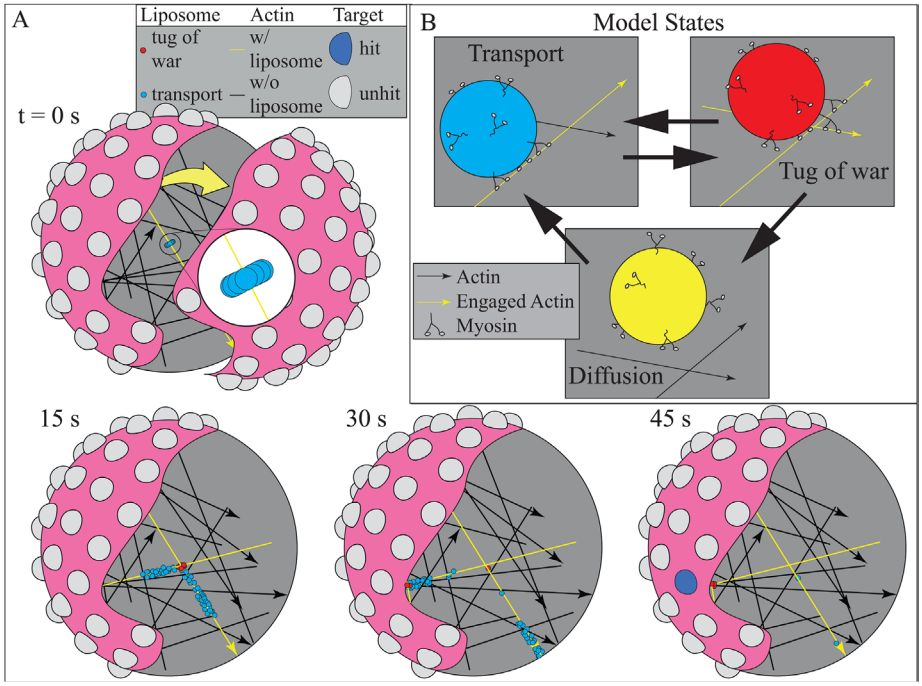

FIGURE 1: Schematic of the simulations. (A) A random mesh of actin filaments span a spherical region (partially cut away for visualization purposes) of radius 10 *μm* (magenta). Fluid liposomes, of 350 nm diameter, are transported (blue) by 10 myoVa motors, undergo tug-of-wars (red), or diffuse according to a coarse-grained model. 2–*μm* diameter spherical targets (gray) are distributed evenly over the surface of the sphere, and are hit (blue) if touched by a liposome. A simulation of 100 liposomes navigating a network of $N = 25$ actin filaments is shown (see Supplemental Movie S7 for a movie of the simulation). Actin filament thickness is exaggerated for visualization purposes; arrows indicate filament plus ends. (B) Schematic of state transitions in the model. Liposomes in the transport state (blue) have myoVa motors engaged with a single actin filament. If a motor engages with a second actin filament, a tug-of-war (red) is initiated. Tug-of-wars may be resolved with motors remaining engaged with the original filament (straight outcome), switching to the new filament (turn outcome), or detaching. In the latter case, the liposome enters the diffusion state (yellow). The coarse-grained model used in our simulations does not keep track of the myoVa motors, but is validated by simulations of a more detailed model that does. In both A and B, actin filaments turn yellow once engaged by a liposome.

thus rarely engage in a tug-of-war (red liposome in the supplemental movies and Figure 1B). By contrast, at high actin density (100–800 filaments; Supplemental Movies S5 and S6) most every liposome was within reach of multiple actin filaments and thus switched between transport and tug-of-war states (red liposome in Figure 2C), resulting in random walk-like trajectories as liposomes often switched filaments once the tug-of-war was resolved (Figure 2C). This apparent change from primarily long-range, directed transport to more circuitous trajectories with increasing actin filament density suggests that network density triggers a shift in the liposome state distribution. Plotting the coarse-grained model state distributions as function of actin density confirms (Figure 3) that the transport state predominates at low actin density, transitioning to a mixture of transport and tug-of-war states with actin densities greater than 50 filaments. Due to multiple motors on the liposome surface being simultaneously engaged with one or more actin filaments, liposomes rarely detached from actin to enter the diffusion state (yellow liposomes in the supplemental movies and Figures 1 and 2A) at any actin density.

To relate how liposome state distributions dictate simulated transport characteristics, motion parameters typically used to describe particle trajectories were determined at each actin density. The average liposome speed (linear distance between initial and final positions divided by simulation time; Figure 4A) remains constant and equal to that for transport along a single actin filament (350 nm/s) at low actin density, but then begins to slow at actin densities >50 filaments to a minimum of 53 nm/s at the highest density (i.e., 800 filaments). This slowing is explained by liposomes transitioning to a mixture of transport and tug-of-war states at high actin densities. The increased frequency of stationary periods during the tug-of-wars and the less-directed trajectories due to filament switching both contribute to the slower average speeds (Figures 2C and 4A).

Another transport descriptor is the mode of trajectory motion, defined by the scaling exponent of the mean-squared displacement (MSD) as a function of time (α_{MSD}), where $\alpha_{MSD} = 0$ for a stationary liposome; $\alpha_{MSD} \sim 1$ for a diffusive-like motion, and $\alpha_{MSD} = 1.8$ for purely directed, straight line motion based on simulations (note that $\alpha_{MSD} < 2$ for directed motion because liposome trajectories are not straight lines, but rather spirals, and because the model is stochastic in terms of both reaction times and step size; see SM). Therefore at each actin density we calculated α_{MSD} for the entire simulated trajectory of each liposome (Figure 4B; see *Materials and Methods* and SM for details). Liposomes primarily adopt a directed mode on low actin density networks (i.e., <50 filaments) shifting toward a more diffusive-like mode at higher densities to a minimum of $\alpha_{MSD} = 1.34$ at the highest density (i.e., 800 filaments). This decrease in α_{MSD} is consistent with the transitions in the liposome state distributions described above, with stationary tug-of-wars and a loss of directionality due to filament switching contributing to the overall motion appearing more diffusive-like; however, calculating α_{MSD} over the entire trajectory averages together times when an individual liposome might adopt different modes of motion. Calculating α_{MSD} over a much shorter time scale (1 s) shows that on the dense actin networks (i.e., >50 filaments), liposomes adopt a mixture of directed and stationary modes of motion (see SM), which directly reflects the transitions in the transport state distributions described above. Thus this shift in liposome motion with actin density is emphasized both in the average α_{MSD} for the entire trajectory and in the standard deviation (SD) of the α_{MSD} calculated over 1 s of the trajectory (Figure 4C), where a small SD indicates a single predominant mode of motion, while a large SD indicates a mixture of modes.

Metric for quantifying global liposome transport

Simulations described above identified a transition in transport characteristics as actin network density increased. However, these motion parameters are average characteristics that describe the transport of a single liposome. If myoVa intracellular transport is potentially associated with cargo delivery to targeted locations, then

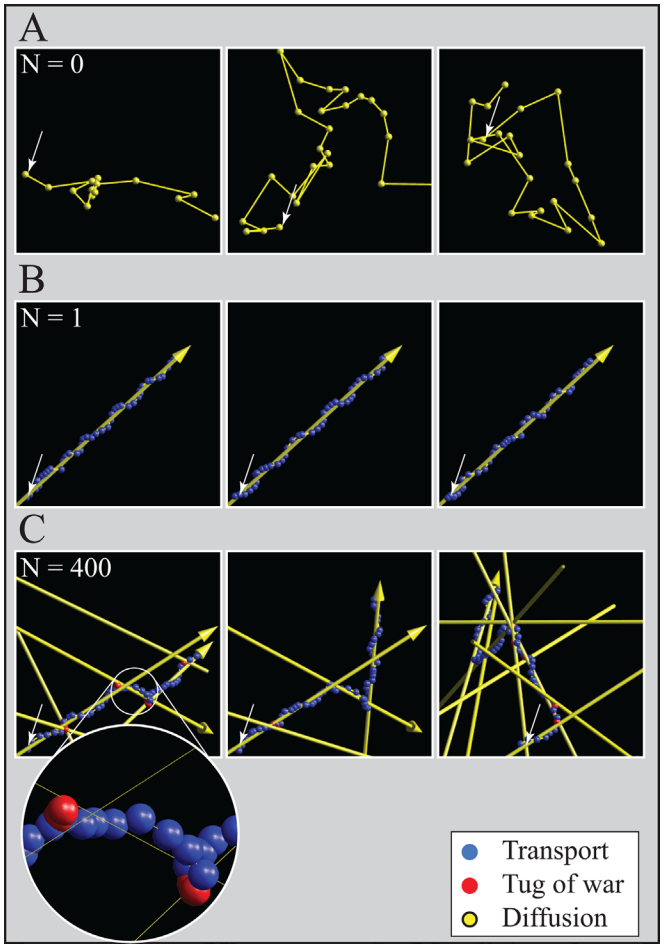

FIGURE 2: Increasing actin network density causes a change in liposome motion. In each panel (A–C), to show the variability of liposome trajectories, three liposome trajectories are shown on the same actin network. Only actin filaments engaged by the liposome are pictured in panels B and C. A. Liposomes in the diffusion state (yellow spheres) describe a random walk. This is rarely observed in our simulations at any actin density. (B) Liposomes transported along a single actin filament (yellow arrow with arrow head indicating plus-end) adopt the transport state (blue spheres). This is observed in our simulations at low actin density. (C) At high actin density, liposomes transition between transport (blue spheres) and tug-of-war (red spheres) states, resulting in a random walk as they switch actin filaments once the tug-of-war is resolved. Actin filament thickness is exaggerated for visualization purposes (the magnification call-out in C shows actual size). Liposome position is shown at equally spaced intervals of $\Delta t = 0.75$s, and Gaussian random noise of SD σ =10 nm is added for visualization purposes. Small white arrows indicate liposome starting position.

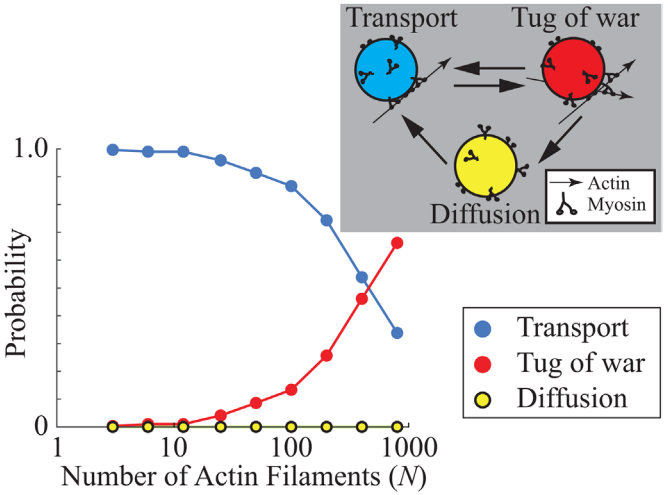

FIGURE 3: Actin network density triggers a shift in liposome state distribution. The average state of a simulated liposome shifts from being almost exclusively transport at low actin density to a mix of transport and tug-of-war at higher density. There is very little diffusion at any density. Inset shows a diagram of the model states and transitions. Error bars (SEM) are smaller than the symbols.

this shift in trajectory motion characteristics with actin filament density may be a regulated cellular property that can modulate targeted cargo delivery. Whether transport is considered targeted for a given network is best described as a property of a liposome population rather than of a single liposome. We, therefore, defined a metric for targeted liposome delivery by evenly spacing 100 spherical (1 μm radius) "targets" on the network boundary surface (Figure 1A). This spatial distribution translates into 35% of the total boundary surface being composed of target sites that can be "hit" by a delivered liposome. Thus at sparse actin filament densities where liposomes may travel from the network center to the network boundary along a single actin filament, the probability of hitting a target is 0.35 on average. In contrast, at higher filament densities, where a multitude of potential paths from the network center to the surface are available, then most, if not all, of the 100 targets may be hit. Thus the smaller the number of targets hit, the more directed the transport on a given network. This metric of liposome transport (i.e., targets hit) provides a simple quantifiable measure for how a liposome population would be delivered within a given actin filament network so that changes to liposome delivery can be readily detected as a result of variations in actin filament density and liposome diameter.

Liposome transport undergoes a phase transition at a critical accessible actin filament density

Model simulations demonstrate that as actin filament density increases, so too does the number of targets hit (Figure 4D). This relationship is best described by two different power laws, which are apparent by plotting the data on a log-log scale. Specifically, at low density, the number of targets hit increases slowly, while increasing more rapidly at higher density (Figure 4D) until deviating at the highest actin filament density (i.e., 800 filaments), where liposome motion is so slow (see above, Figure 4A) that liposomes generally do not reach the network boundary during the 100 s simulation. The presence of two scaling regimes suggests a phase transition. In fact, all properties of transport we measured show a change in scaling that occurs at a critical actin density, $N_c \approx 60$ filaments, defined as the x intercept of the fit to the second phase (Figure 4, A–D). This phase transition may be related to the number of actin filaments accessible to liposome transport.

The number of accessible actin filaments is a geometric property of a given actin network. To be considered accessible to a liposome traveling along an actin filament, a second actin filament must be in reach of motors on the liposome surface. After simulating all potential paths that a liposome could traverse from its start at the network center to the network boundary without detaching from actin, this set of filaments was defined as the number of accessible actin filaments for a given network (see SM for more details and Figure 4F for examples). The number of accessible actin filaments as a function of

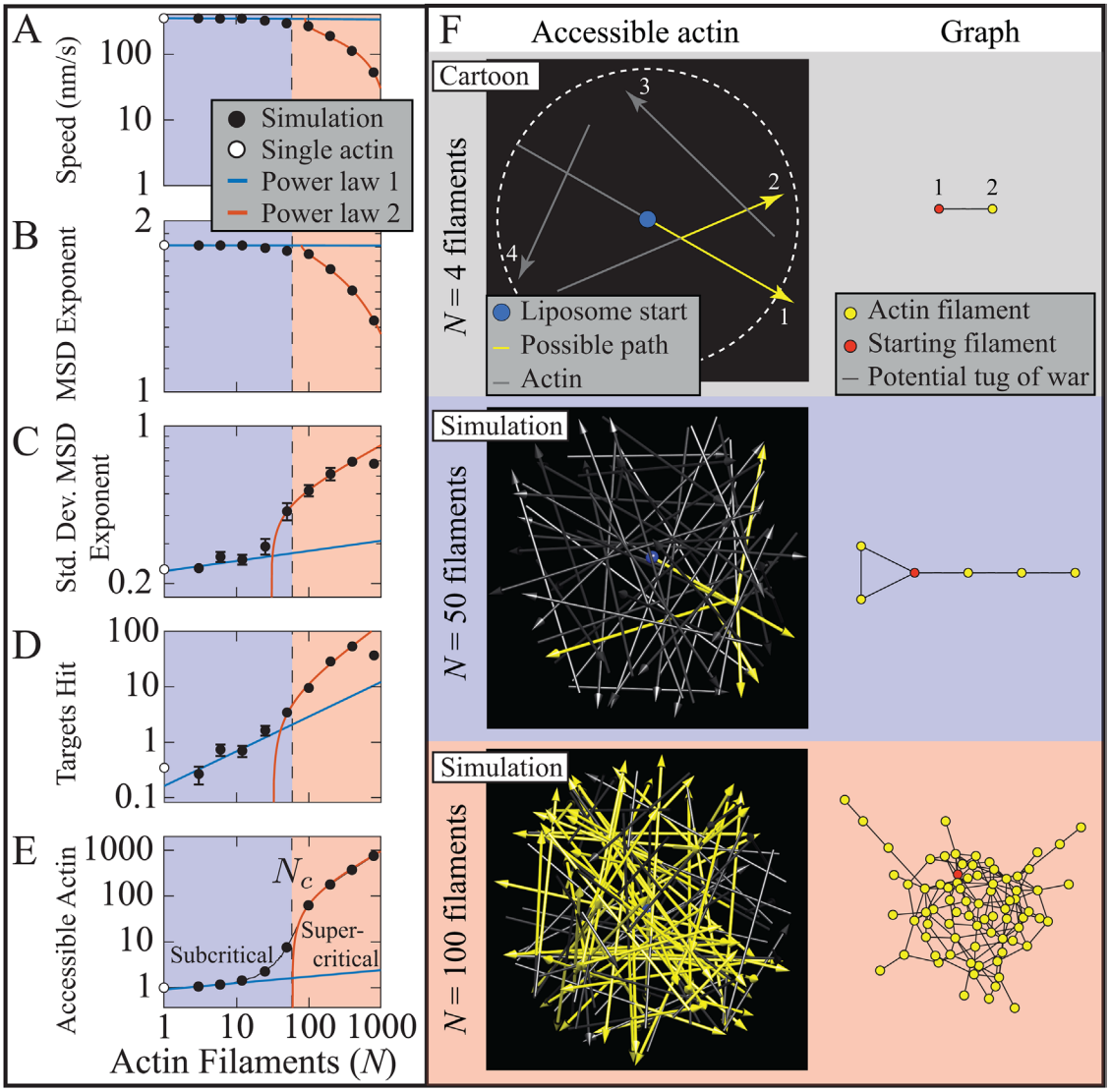

FIGURE 4: A change in the number of actin filaments accessible for transport underlies a phase transition in myoVa-based transport with increasing actin density. Different quantities for liposome motion, i.e., liposome speed (A), MSD exponent (B), SD of MSD (C), and number of targets hit by liposomes at the network boundary (D) show a change in scaling as best described by two different power laws similarly to the change in scaling that occurs in the number of accessible actin, $N_c \approx 60$ actin filaments (E) (see text for details). The blue-shaded region is where power law 1 applies, and the red-shaded region is where power law 2 applies for the accessible actin. Error bars show SEM. White circles show values for a single actin filament. Schematics of accessible actin (F), represented as the number of potential transport paths on a given actin network (left), and as a graph (right). Top shows a cartoon with 4 actin filaments as a demonstration. In this network, actin filaments 1 and 2 are within reach of a myoVa on the liposome surface, r_B (i.e., distance from liposome center to the tip of myoVa on the liposome surface; see SM for details), at their nearest point, while actin filaments 1 and 3, and 2 and 3 are further than r_B. Actin filament 4 is not accessible even being closer than r_B to filament 1 due to the liposome starting at the center of filament 1 and then travels toward the plus-end away from filament 4. A much greater percentage of the actin filaments are accessible for the larger network ($N = 100$ filaments, 78/100=78%) than for the smaller network ($N = 50$ filaments, 6/50 = 12%). In each graph (right), accessible actin filaments are shown as vertices (yellow circles, starting filament as red circle), and potential tug-of-wars as edges (black lines). Actin filament thickness is exaggerated for visualization purposes; arrow heads indicate plus-ends; see Supplemental Movies S8 and S9 for simulations of liposomes transported through the two networks. Power law fits are for the various relationships in panels A–E: power law 1, 350 N^0 (A), 1.8 N^0 (B),0.23 $N^{0.05}$ (C), 0.16 $N^{0.63}$ (D), 0.91 $N^{0.14}$ (E); power law 2, 350–42(N–90)$^{0.30}$ (A), 1.8–0.011(N–79)$^{0.57}$ (B), 0.25(N–30)$^{0.18}$ (C), 0.21(N–32)$^{0.94}$ (D), 2.6(N–60)$^{0.86}$ (E).

total number of actin filaments within the network is also described by two different power laws (Figure 4E). The transition between these two phases occurs at the same actin filament density, i.e., $N_c \approx 60$ filaments, as for the other transport properties (Figure 4E). Therefore at actin densities below this critical number ($N < N_c$), the number of accessible actin is small with few potential paths for liposome transport (Figure 4E) so that liposomes are predominantly in the transport state (Figure 4), whereas above this value ($N > N_c$), the number of accessible actin increases rapidly, resulting in numerous, complex transport paths due to a mixture of transport and

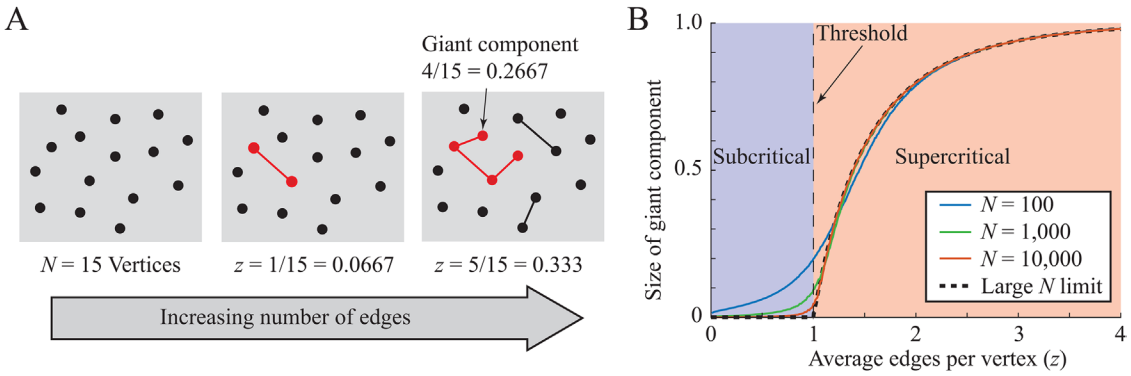

FIGURE 5: A schematic of a percolation phase transition on a network with random connections. (A) A cartoon of $N = 15$ vertices (black circles), with an increasing number of edges, where an edge (line) connects two vertices. The giant component is the largest number of edge connected vertices (red circles and lines). z equals the average number of edges per vertex within the network. (B) Plot of the size of the giant component as a proportion of the total number of vertices versus z for networks with different numbers of vertices, N. As N approaches infinity, the size of the giant component becomes nonzero above a critical number of edges, the percolation threshold, and networks switch from being subcritical to supercritical.

tug-of-war states (Figure 3) that culminate in random walk-like trajectories (Figure 2C). Therefore the phase transition in the number of targets hit is a direct reflection of the network geometry, i.e., a phase transition in the number of accessible actin filaments and potential paths as the liposome weaves its way through the network. Here we show that this geometric phase transition is a percolation phase transition described in graph theory and physics.

A percolation phase transition in the actin network underlies the phase transition in liposome transport

Percolation phase transitions, originally defined in the context of water draining through a porous medium (Broadbent and Hammersley, 1957), occur in a broad range of discrete networks including the internet (Cohen *et al.*, 2001), power grids (Solé *et al.*, 2008), epidemics (Newman and Watts, 1999), liquid-to-gel phase transitions in polymers (Stockmayer, 1943; Flory, 1953; Stauffer, 1976; Coniglio *et al.*, 1979), and actin networks in the presence of cross-linking proteins (Alvarado *et al.*, 2013). Common to all of these systems, and potentially the liposome transport system described here, is that a phase transition (i.e., a change in power law scaling) arises from a sudden increase in overall network connectivity as connection probability increases. As a demonstration of this process, consider a graph representing a network with N vertices and a line that connects a pair of vertices termed an edge (Figure 5A). As additional edges connect pairs of vertices chosen at random, the average edges per vertex for the network, z, increases linearly from 0. However, the size of the giant component, i.e., the largest number of vertices that form a connected cluster as a fraction of N (Figure 5A), varies discontinuously with z (Figure 5B). When z is small, the giant component makes up a negligible fraction of the total number of vertices (Figure 5B). Such a network is said to be *subcritical*. Beyond a critical z value, the percolation threshold, the giant component makes up a nonnegligible fraction of the vertices and rapidly increases until all vertices are connected. Such a network is said to be *supercritical*. As the size of the network N increases, this phase transition becomes sharper and, in the limit of an infinitely large N, shows a discontinuity in slope at the percolation threshold, N_c (Figure 5B). Though networks can differ in their details, all percolation phase transitions arise from a sudden increase in network connectivity, measured in the above example as the size of the giant component, which underlies different power law scaling on subcritical and supercritical networks.

Assuming the transport characteristics of our modeled liposome transport system are reflective of a percolation phase transition, each actin filament can be represented as a vertex and an edge, as a tug-of-war, connecting two vertices (i.e., separate actin filaments) due to the filaments being spatially close enough so that myoVa motors on the same liposome can simultaneously interact with both filaments (Figure 4F). Increasing the number of actin filaments in the network, N, adds vertices and with each additional vertex the potential for an edge (i.e., tug-of-war) increases. If our system undergoes a percolation phase transition, then we expect to see a critical actin filament density, N_c, above which a nonnegligible fraction of the total vertices creates a connected cluster and forms the giant component. That is, above N_c a liposome starting on a filament at the network center could potentially reach a nonnegligible fraction of the other actin filaments without having to detach and undergo diffusion. This quantity is what we have called the accessible actin. The fact that there is a change in scaling at $N_c = 60$ filaments for not only accessible actin but also each transport property we measured (Figure 4, A–D) suggests that there is a phase transition in liposome transport within these networks that arises from a percolation phase transition in the actin network. However, the discontinuity at this threshold is not as sharp as might be expected (see Figure 5B).

To better identify the percolation threshold, N_c, by a clear discontinuity in the number of accessible actin filaments, we accounted for two factors that contributed to smoothing of this phase transition in Figure 4E. The first of these factors is stochastic effects introduced by the random placement of filaments within each network. Therefore we generated 10,000 different actin networks at each actin density below and above the N_c estimated from Figure 4E. A histogram of the accessible actin as a proportion of the total actin on subcritical networks with $N < N_c$ (e.g., $N = 35$, Figure 6A) shows a single peak at the most common condition: a single accessible actin filament. This single accessible actin filament is the actin filament on which the liposomes start, and trajectories along 2, 3, or more actin filaments are increasingly rare (Figure 6A). However, as the network density crosses N_c (e.g., $N = 70$, Figure 6B), the distribution of the accessible actin as a proportion of the total actin becomes bimodal, with multiple accessible

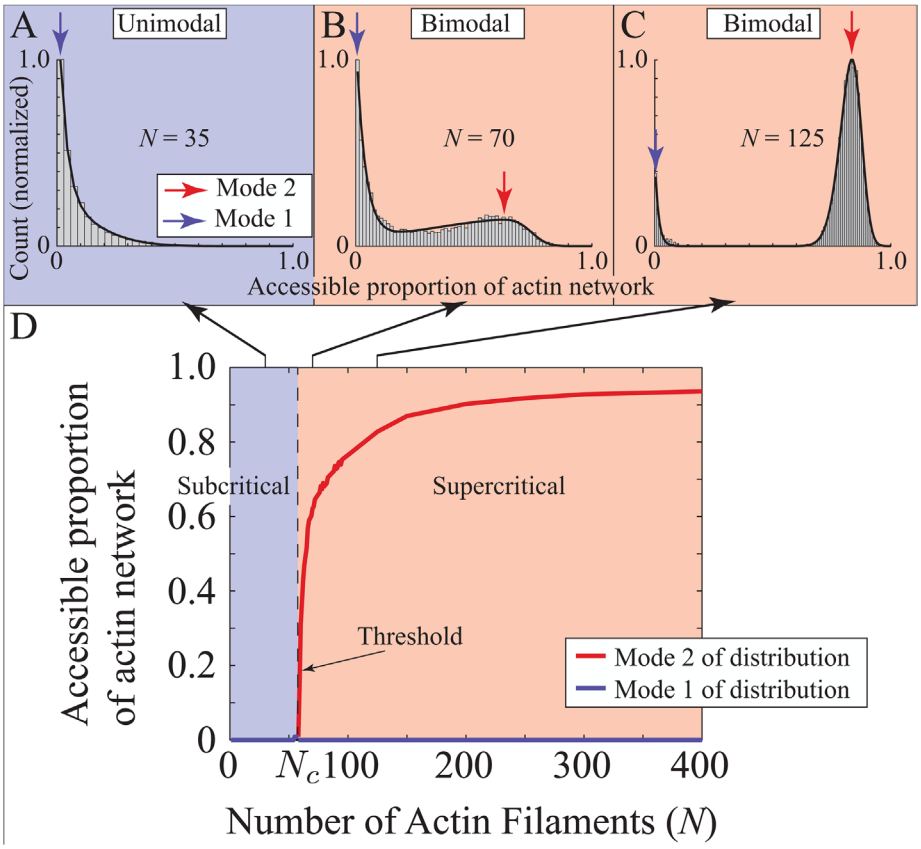

FIGURE 6: Percolation in accessible actin. (A–C) Histograms of the proportion of accessible actin within 10,000 networks for various network densities. On a subcritical network (A, $N = 35$), the histogram has a mode of 1. On a supercritical network (B and C, $N = 70$ and 125, respectively), the histogram is bimodal. (D) Plotting the mode(s) of the distribution as a function of the number of actin filaments shows the percolation threshold, $N_c = 58$, and the transition from subcritical to supercritical networks. Note that to calculate the accessible proportion of the actin network, we subtract 1 from accessible actin and divide by the total number of filaments.

actin filaments becoming more common, though a single accessible actin filament can still occur. Finally, at large supercritical network densities (i.e., $N > N_c$, e.g., $N = 125$, Figure 6C), the bimodal distribution is distinct, with a minor component at a single accessible actin filament still apparent. This bimodal distribution for supercritical network densities arises because the accessible actin must include the actin filament where transport starts. Due to the stochastic nature of each actin network, the starting actin filament may not be part of the network's giant component. A single accessible actin filament is therefore possible, leading to the existence of a minor component of the distribution, i.e., mode 1. For each actin network density, N, the distributions of the accessible actin cluster size as a proportion of network density (Figure 6, A–C) were determined and these distributions fitted to define the mode(s) (see SM). By plotting these mode(s) of the fit versus N (Figure 6D), an abrupt transition exists at the percolation threshold $N_c = 58$, where the actin network transitions from subcritical actin densities with predominantly single actin filament transport to supercritical actin densities where transport is on connected actin filament clusters (Figure 6). This precise estimate of N_c supports our previous assumption that the apparent phase transition in the number of targets hit and accessible actin filaments that we estimated at $N_c = 60$ is a network property that reflects a percolation threshold and underlies transitions in all of the metrics used to describe liposome transport (Figure 4, A–D) as well as the liposome state distributions (Figure 3).

Actin network percolation threshold is dependent on both liposome diameter and travel distance

The percolation threshold for liposome transport described here is a geometric property of the network system that involves an interplay between actin network density and liposome diameter. Can the percolation threshold be predicted for any diameter liposome being transported over some distance through an actin filament network? A detailed analysis (see SM) gives a nearly linear scaling of the percolation threshold N_c with the transport distance, d_T, divided by liposome radius plus motor reach, r_B, i.e., $N_c = k\,(d_T/r_B)^{0.9}$, where k is a proportionality constant. The value of k can be estimated as 1.8 based on our predicted $N_c = 58$ from simulations for a 350 nm diameter ($r_B = 210$ nm) liposome traveling 10 μm from its starting point at the network center. Therefore a generalizable relationship for N_c is $N_c = 1.8\,(d_T/r_B)^{0.9}$.

We can understand this near-linear scaling by considering a graph with edges connecting randomly selected vertices which, as illustrated in Figure 5, undergoes the percolation phase transition when vertices, on average, have one edge ($z = 1$, Figure 5B). In our simulations, vertices correspond to actin filaments and edges to potential tug-of-wars that occur only if motors on the liposome surface are within reach of nearby actin filaments (Figure 4F). Thus the percolation threshold (N_c) is the network density at which a liposome traveling on an actin filament will encounter, on average, one other actin filament and engage in a tug-of-war, which is repeated as the liposome meanders from actin filament to actin filament. The percolation threshold should therefore occur when actin filaments, on average, are spaced about a liposome diameter apart, $2r_B$. In silico modeling (see SM) predicts that the 3D spacing between filaments scales inversely with the filament number, N, and is directly proportional to the transport distance, d_T (Supplemental Figure S5A). So, at the percolation threshold, we predict $2r_B = c(d_T/N_c)$, where c is a proportionality constant. This gives a linear scaling of the percolation threshold, N_c, with d_T/r_B. The actual scaling, as described by the generalized equation above, is slightly less than linear because graphs generated from actin networks are not exactly random; instead, the probability of a potential tug-of-war decreases as the liposome switches actin filaments, with the amount of decrease weakly dependent on d_T/r_B (see SM for details).

To test this predicted scaling of N_c, we ran a second set of simulations with fivefold larger liposomes, $r_B = 910$ nm (see SM for details), with $N_c = 1.8(10{,}000\text{ nm})/(910\text{ nm}) = 15$ predicted as the percolation threshold. By estimating the percolation threshold as before through histograms of the accessible actin as a proportion of a given actin network (Figure 6), $N_c = 11$ filaments (Figure 7A). This 5.3-fold decrease in N_c compared with that for 350-nm diameter liposomes

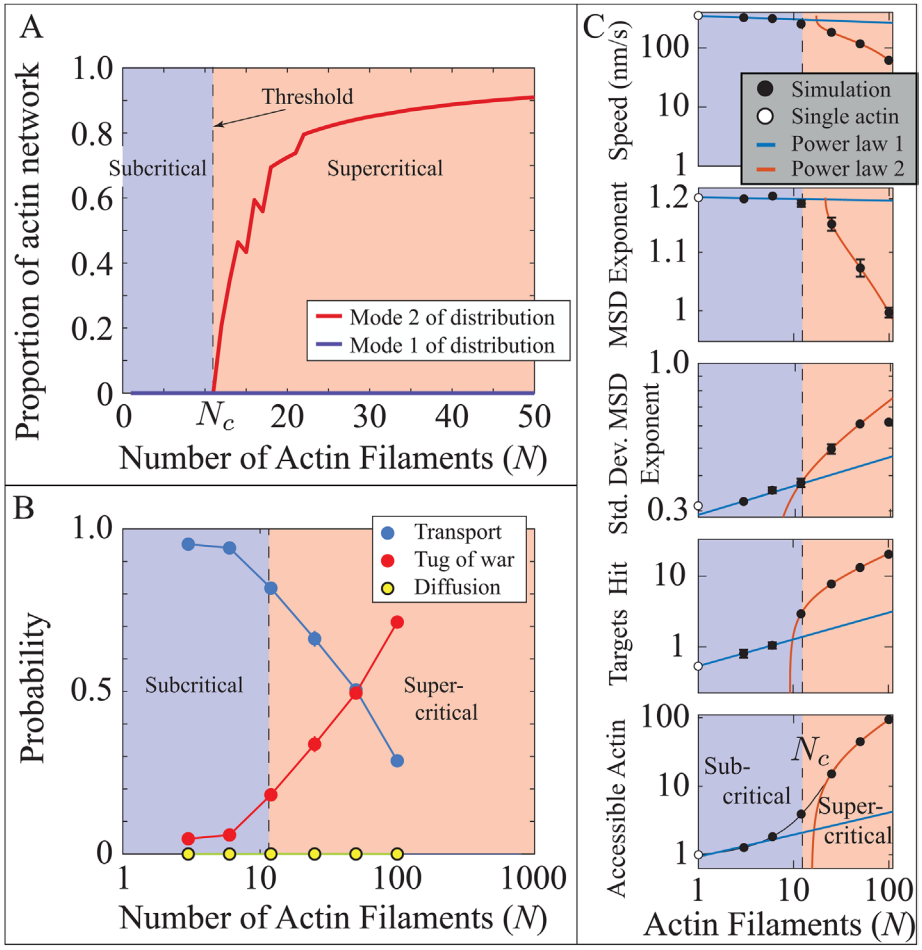

FIGURE 7: A fivefold increase in liposome size decreases the percolation threshold N_c, and the transition between scaling regimes, by a factor of five. (A) Histograms of accessible actin as a proportion of the total number of actin filaments within the network switch from being unimodal to bimodal at a critical network size of N_c = 11 filaments (see Figure 6). (B) The average state of a simulated liposome shifts from being almost exclusively transport to a mix of transport and tug-of-war as the number of actin filaments increases past N_c. Error bars (SEM) are smaller than the symbols. (C) Different quantities describing liposome motion (described in detail in main text) show a change in scaling similar to that which occurs in the number of accessible actin (bottom graph). White circles show predicted values for a single actin filament. Each transition occurs at a network size roughly fivefold less than for smaller liposomes (see Figure 6). Error bars show SEM. Power law fits in C are: power law 1, 350 $N^{-0.06}$ (Speed), 1.2 N^0 (MSD exponent), 0.28 $N^{0.13}$ (SD MSD exponent), 0.88 $N^{0.38}$ (Targets Hit),0.94 $N^{0.32}$ (Accessible Actin); power law 2, 350–100(N–17)$^{0.23}$ (Speed), 1.20–0.029 (N–22)$^{0.45}$ (MSD exponent), 0.24 (N–5.8)$^{0.24}$ (SD MSD exponent), 2.8(N–9.4)$^{0.55}$ (Targets Hit), 2.4 (N–15)$^{0.83}$ (Accessible Actin).

is in reasonable agreement with the predicted N_c = 15 from the generalized equation above. The liposome diameter-dependent shift in N_c was similarly reflected in a ~5-fold lower actin density at which phase transitions occurred for the coarse-grained model state distributions (Figure 7B) and all other transport descriptors (Figure 7C). These results confirm that the percolation threshold, N_c, scales inversely with cargo diameter and underlies the phase transitions in liposome transport (see SM for further analysis), specifically from directed motion in subcritical networks to random walk-like motion interspersed with stationary pauses in supercritical networks.

Liposome diffusion and its impact on transport outcomes

In simulations described above, we observed liposome trajectories in supercritical actin networks with MSD exponents approaching 1 (Figures 4B and 7C). This diffusive-like mode of motion arises from liposomes being transported along a sequence of randomly oriented actin filaments (Figures 4 and 7B). In simulations at all actin densities, true diffusion is rare because there are sufficient motors on the liposome to engage one or more actin filaments so that liposome detachment does not occur. In a cell, however, diffusion may be initiated by deactivation of motors, the presence of actin-binding proteins that cause myoVa motors to detach, or myoVa-bound cargoes being assembled far from the actin network so that myoVa motors cannot engage. Therefore we performed simulations as described above, but with liposomes starting at the network center unbound to actin (see Supplemental Movies S10–S14).

As expected, on the lowest actin density networks (N < 50 filaments), liposomes were predominately in the diffusion state (Supplemental Figures S8 and S9D; SM). However, on networks with N > 50 filaments, the model state distribution becomes nearly identical to simulations where liposomes start bound to actin (see SM). This transition from the diffusion state to a mixture of transport and tug-of-war states corresponds to the percolation threshold (N_c = 58). This, however, is a coincidence, since this transition does not correspond to the percolation threshold for the larger liposomes (r_L = 875 nm; Supplemental Figure S9E; SM).

DISCUSSION

MyoVa transport of vesicular cargo along the cell's actin cytoskeletal network involves a complex interplay between motors on the cargo surface that power cargo movement, the cargo dimensions, and the spatial arrangement of the actin filament tracks on which transport occurs. These three components (i.e., motors. cargoes, tracks) can vary significantly among cell types and even within a cell, as physiological demands warrant. With all three components potentially regulated, the cell then possesses a highly tunable cargo transport and delivery system. However, defining how each transport component contributes to cargo delivery requires investigators explore an enormous parameter space within cells that is experimentally challenging. To avoid these complexities, we developed a coarse-grained in silico model of liposome transport by myoVa motors within complex networks of randomly arranged actin filaments. Liposome movement transitions between three states of motion described as transport, tug-of-war, or diffusion, with the distribution of these states varying with actin density. Specifically, as actin density increases, liposomes transition from the highly directed "transport" state along single actin filaments to one described as a random walk, as the probability of a liposome encountering another filament increases and the motors on the liposome surface engage in a tug-of-war, with the resultant outcome a potential change in

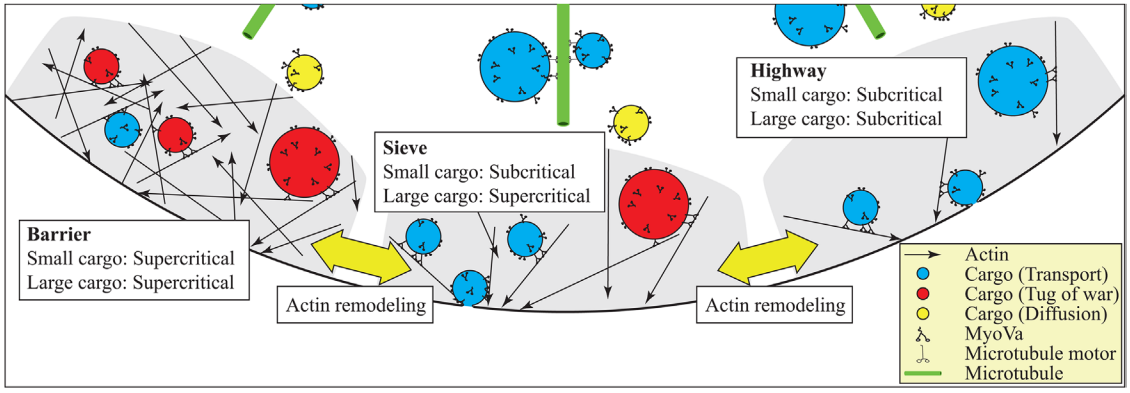

FIGURE 8: By varying actin density, cells can switch the functional role of the actin network to regulate intracellular transport.

travel direction. This transition in transport characteristics arises from a percolation phase transition in the number of accessible actin filaments (Figures 4E and 6D), which is a geometric property of the actin network that depends only on the position and polarity of the actin filaments, transport distance, and the liposome diameter. Interestingly, this percolation phase transition is predictive of phase transitions in various metrics of liposome transport that occur at the same actin density as the percolation threshold.

Percolation transition in liposome transport through actin networks

Percolation transitions have been described previously in cytoskeletal networks in which the network consisted of actin filaments, actin filament cross-linking proteins, and myosin-II motor filaments. In these systems, transitions in the network's macroscopic properties (e.g., the fluid-to-gel-like transition reviewed in Alvarado *et al.*, 2017) depend on actin cross-linkers creating actin network connectivity so that myosin-II motor-generated forces are transmitted some distance within the network beyond where force originates. Phase transitions in motor-driven transport have been observed in these network systems as well. For example, some studies have found that trajectories of myosin-II filaments transition from directed motion to becoming trapped in rings of actin filaments as the amount of cross-linking protein is increased (Scholz *et al.*, 2016, 2020). Other studies have found that with enhanced actin filament connectivity due to the addition of cross-linking proteins, directed myosin-II filament motion transitions to being stationary, as the motors undergo force-dependent stalling while engaged with separate actin filaments (Jung *et al.*, 2019). Although our liposome transport model similarly identifies actin filaments as vertices in a network, edges connecting these vertices are not physical cross-links as in the studies described above but rather locations where a tug-of-war might occur as myoVa motors on the liposome surface engage separate actin filaments. Thus in our model percolation does not underlie a phase transition in the mechanical properties of the actin network but instead underlies the phase transition in the transport properties of the myoVa-liposome system. This phase transition involves both changes in motor trajectories, as they go from directed on subcritical networks to random walks on supercritical networks and, concurrently, a sudden increase in the number of stationary liposomes as tug-of-wars become much more probable. The existence of phase transitions in transport has implications in the regulation of intracellular transport, i.e., small changes in actin density or liposome diameter can have profound effects on motor-driven cargo transport.

Actin network form and function

In cells, both spatial and temporal variations in the cytoskeletal actin density may provide a mechanism to control the functional role that the actin network adopts (i.e., highway, sieve, or barrier; Figure 8) through its impact on vesicular transport generated by the myoVa motors on the cargo surface. Therefore the cell might exploit actin network transitions between subcritical and supercritical actin densities as a means of switching actin network functional roles thereby dictating cargo transport outcomes. For example, on sparse, subcritical actin networks, regardless of cargo size, the actin network would behave as a highway for directed and potentially targeted cargo delivery (Figure 8). However, the percolation threshold for a given actin network does vary inversely with cargo radius, so that larger liposomes experience a transport phase transition at lower actin densities. Thus a given actin network could act as a transport "sieve" (Figure 8), whereby larger liposomes would get frequently caught up in tug-of-wars, while smaller liposomes would move relatively unencumbered to their targets along actin filaments (see SM for an example). Finally, at supercritical actin densities, the actin network may serve as a "barrier" (Figure 8) as cargo and their myoVa motors transition predominantly to the tug-of-war state (Figures 3 and 7B).

This latter condition, where the actin networks act as a barrier, has been described for insulin granules that are believed to exist in a readily releasable pool near the cell membrane within the dense cortical actin network (Rorsman and Renström, 2003; Porat-Shliom *et al.*, 2013). Consistent with this, we would predict that a ~200-nm insulin granule (r_B = 100 nm) transported ~1 μm (d_T = 1000 nm) would have a percolation threshold of ~14 actin filaments. Using our scaling law that applies to random actin networks $N_c = 1.8(d_T/r_B)^{0.9}$, this corresponds to a density of ~4.4 μm actin/μm^3, or ~2.9 μM. Measurements of actin networks in cells have a density around five times this value, suggesting that the actin network, if random, would act as a barrier to transport (Heaslip *et al.*, 2014). However, our scaling law applies to random actin networks, and actin networks with some orientation bias, or with branching and/or cross-linking proteins that promote specific orientation would have a different scaling law. Our own work suggests that the branching protein Arp2/3 can promote directed transport (Lombardo *et al.*, 2019). This barrier to granule delivery and docking to the cell membrane may therefore be eliminated on glucose stimulation by the regulated activity of actin severing (e.g., cofilin) and branch-forming (e.g., N-WASP/Arp2/3) proteins, creating a more favorable, subcritical density of actin filaments for myoVa granule delivery. This transition from myoVa being a tether to transporter further emphasizes the role

that the actin filament network and its dynamic structure plays in cargo transport.

In the future, building further complexity in vitro will require understanding of how cargo decorated with both actin- and microtubule-based motors share their transport duties in mixed cytoskeletal networks composed of both actin filaments and microtubules. Nevertheless, the modeling approach outlined here will allow these transport systems to be efficiently and accurately described over physiologically relevant spatial and temporal time scales.

MATERIALS AND METHODS

Coarse-grained model

We developed a coarse-grained version of our experimentally validated model for the transport of fluid, 350 nm (radius $r_L = 175$ nm) liposomes by a team of 10 myoVa motors through 3D actin networks (Lombardo *et al.*, 2017, 2019). This coarse-grained model does not keep track of the myoVa motors on a liposome and their force and motion generation; instead, at any given time, the liposome is assigned to one of three states: 1) transport, where one or more motors are engaged with a single actin filament; 2) diffusion, where no motors are engaged with an actin filament; or 3) tug-of-war, where some motors are engaged with one actin filament and other motors are engaged with a second actin filament. When in the transport state, the liposome moves along an actin filament toward the filament plus-end with a 36-nm step 78% of the time and with a short 31-nm step 22% of the time. Due to the helical arrangement of binding sites on the actin filament with a repeat distance of 36 nm, the liposome moves along an actin filament in a spiral path with an average period similar to experimental measurements (Ali *et al.*, 2002; Lombardo *et al.*, 2017). When the liposome encounters a second actin filament within reach of the motors ($r_B = 210$ nm from the liposome center, a parameter of the coarse-grained model determined from fitting simulations of our detailed model and includes the liposome radius r_L =175 nm and the motors' effective reach; see SM), the liposome may enter the tug-of-war state where it becomes stationary. The tug-of-war is resolved when one of the motor teams generates a greater force allowing the liposome to enter the transport state on the actin filament associated with the winning team. A tug-of-war can also resolve by all motors detaching from actin and the liposome entering the diffusion state. In the diffusion state, the position of the liposome is determined at time intervals of $\Delta t = 0.5$ ms. The liposome takes a random step in (x, y, z) from a Gaussian distribution with SD $\sigma_D = \sqrt{2D\Delta t}$ (for the radius $r_L = 175$ nm liposomes, with diffusion constant $D = 1.3$ μm^2/S, this is $\sigma_D = 36$ nm). From the diffusion state, the liposome can enter the transport state when it collides with an actin filament. The small time step ensures that the simulation does not miss these collisions when they occur.

Transitions between states and stepping are determined by rate constants that depend on the proximity of actin filaments to the liposome, whereas the tug-of-war duration is dependent on the position and polarity of the two actin filaments with which the motors are engaged. These state transitions are determined with a Monte Carlo method using a modified version of the Gillespie algorithm (see SM for details). The rate constants governing the state transitions and the reach of the motors (r_B) were determined by fitting the coarse-grained model to thousands of simulations of our more detailed model (Lombardo *et al.*, 2017, 2019) (see SM for the fits). Since the Gillespie algorithm takes time steps of variable size and our simulation of diffusing liposomes takes constant time steps, the algorithm records liposome position and state at the constant time step and, when a state transition occurs between time steps, the new state is updated at the following time step (see SM for details).

Liposome transport through a random actin network

We used this model to investigate how the density of actin filaments placed randomly in a network bounded by a 20 μm sphere affects 350 nm (radius, $r_L = 175$ nm) liposome transport. Each liposome starts at the network center bound to an actin filament. Therefore one of the actin filaments in the network was constrained to pass through the center of the network sphere. For ease in modeling, the remainder of the actin filaments are placed randomly inside a $10 \times 10 \times 10$ μm cube within the sphere. Their placement is accomplished by randomly selecting two points in the cube. An actin filament then connects those two points and extends in both directions to the network boundary. The actin filament polarity is assigned as the actin minus-end being nearer the first point and the plus-end nearer the second point.

For each actin network, we simulated the motion of 5000 liposomes. Each simulated liposome trajectory concludes when either the liposome reaches the network boundary or 100 s elapse, whichever happens sooner. We performed these simulations on actin networks of 3, 6, 12, 25, 50, 100, 200, 400, and 800 filaments covering roughly three orders of magnitude. For the networks with fewer filaments (3, 6, 12, 25, 50, 100), which typically gave more variable results, we examined $n = 30$ randomly generated networks. For the networks with more filaments (200, 400, 800), which gave more consistent results and were more computationally expensive, we examined fewer networks ($n = 15$, 8, and 5, respectively).

Analysis of liposome trajectories

The output of each simulation was: 1) the 3D position and model state of each liposome at 0.0005 s intervals over ≤100 s; 2) the position and polarity of each actin filament. The position and state matrices being at least 5000 liposomes by 200,000 time points were too big to store and analyze easily. Therefore after each simulation, matrices were compressed by only keeping every hundredth entry, equivalent to a time step of 0.05 s. In this way, we can still take a sufficiently small time step to ensure we don't miss collisions between liposomes and actin yet get simulated data with time steps similar to experimental measurements.

We measured four properties of each liposome trajectory: 1) average model state, 2) average speed, 3) MSD scaling exponent for the entire trajectory, and 4) SD of the MSD scaling exponent calculated over 1 s between $t = 9$ and $t = 10$s of the trajectory. These quantities were calculated as follows. The average model state for a given trajectory was determined as the proportion of simulation time that the liposome spent in each of the three states. For the 5000 liposomes trajectories, the population average state is the average of these probabilities for the individual liposome trajectories. Average speed was the distance between the final and initial position of the liposome divided by total simulation time. MSD scaling exponent was calculated by determining the MSD at a range of times, ΔT, from the time step 0.05 s to half the total simulation time and then calculating the best fit slope of MSD versus ΔT on a log-log scale. To calculate MSD scaling exponent for the entire trajectory, we performed the above calculation on the entire trajectory. For the SD of the MSD scaling exponent, we performed the above calculation between $t = 9$ and $t = 10$ s and obtained the SD of this value for all 5000 liposomes.

Number of hit targets

As a measure of global transport within a given actin network and whether or not such transport could be considered "targeted," we

uniformly distributed 100 2 μm-diameter spherical targets on the network boundary sphere (see SM for details). A target was hit when any part of the liposome surface came into contact with a target. The number of targets hit provides a metric of the spread in the trajectories: if few targets are hit, then the trajectories are all approximately in the same direction; if many targets are hit, then the trajectories go in many different directions.

Accessible actin

The number of accessible actin filaments in a given actin network is the set of potential filaments that can be reached by liposomes as they move from their starting point at the center of the network to the network boundary without detaching from actin (the algorithm, including validation, is given in the SM). This set determination encompasses the multitude of paths taken as a result of filament switching following a tug-of-war and that all paths must be in the direction of the actin plus-end. Therefore not every actin filament will be in the set of accessible actin if access to an intersecting filament requires the liposome to travel toward the minus-end of a filament, which cannot occur.

Simulations with larger liposomes

We performed a series of simulations as described above but with fivefold larger, 1750 nm diameter ($r_L = 875$ nm), liposomes. The liposome diffusion constant was suitably adjusted ($D = 026\ \mu m^2/s$, giving a diffusion step size of σ_D = 16 nm). Additionally, because the parameters of the coarse-grained model change with liposome size, we determined the rate constants governing the model state transitions and the reach of the motors (r_B) by fitting the coarse-grained model to thousands of simulations of our more detailed model (Lombardo *et al.*, 2017, 2019) in the same way as for the smaller liposomes (see SM for the fits).

For the simulations with larger liposomes, we constructed actin networks in the same way as for the smaller liposomes and also simulated the motion of 5000 liposomes. However, we performed the simulations on actin networks of 3, 6, 12, 25, 50, and 100 filaments, covering roughly two orders of magnitude, since the simulations were generally more computationally expensive and to ensure that the pore sizes of the networks were larger than the liposome diameter (see SM). For the networks with fewer filaments (3, 6, 12), which typically gave more variable results, we examined $n = 30$ randomly generated networks. For the networks with more filaments (25, 50, 100), which gave more consistent results and were more computationally expensive, we examined fewer networks (n = 20, 10, and 5, respectively).

Simulations with initially diffusing liposomes

We ran simulations with both small (350 nm, $r_L = 175$ nm) and large (1750 nm, $r_L = 875$ nm) liposomes initially detached from actin and therefore in the diffusion state. Simulations were performed identically as for the case where liposomes start attached to an actin filament, except that we ensured that no actin filament passed through the liposome's initial position. Actin networks were also constructed identically, except we did not constrain one actin filament to pass through the center of the network.

ACKNOWLEDGMENTS

The authors are grateful to Brandon Bensel for helpful discussion and feedback on an early version of the paper. This work was supported by grants from the National Institutes of Health R01GM094229 and R35GM141743 (to D.M.W.) and supported in part by a generous gift to D.M.W. from Arnold and Mariel Goran.

REFERENCES

Ali MY, Krementsova EB, Kennedy GG, Mahaffy R, Pollard TD, Trybus KM, Warshaw DM (2007). Myosin Va maneuvers through actin intersections and diffuses along microtubules. Proc Natl Acad Sci USA 104, 4332–4336.

Ali MY, Uemura S, Adachi K, Itoh H, Kinosita K, Ishiwata SI (2002). Myosin V is a left-handed spiral motor on the right-handed actin helix. Nat Struct Biol 9, 464–467.

Alvarado J, Sheinman M, Sharma A, MacKintosh FC, Koenderink GH (2013). Molecular motors robustly drive active gels to a critically connected state. Nat Phys 9, 591–597.

Alvarado J, Sheinman M, Sharma A, MacKintosh FC, Koenderink GH (2017). Force percolation of contractile active gels. Soft Matter 13, 5624–5644.

Baladanyan V, Arnold DB (2014). Actin and myosin-dependent localization of mRNA to dendrites. PLoS One 9, e92349.

Bendix PM, Koenderink GH, Cuvelier D, Dogic Z, Koeleman BN, Brieher WM, Gield CM, Mahadevan L, Weitz DA (2008). A quantitative analysis of contractility in active cytoskeletal protein networks. Biophys J 94, 3126–3136.

Broadbent SR, Hammersley JM (1957). Percolation processes: I. Crystals and mazes. Math Proc Cambridge Philos Soc 53, 629–641.

Cohen R, Erez K, ben-Avraham D, Havlin S (2001). Breakdown of the internet under intentional attack. Phys Rev Lett 86, 3682.

Coniglio A, Stanley HE, Klein W (1979). Site-bond correlated-percolation problem: a statistical mechanical model of polymer gelation. Phys Rev Lett 42, 518.

Desnos C, Huet S, Darchen F (2007). Should I stay or should I go?: myosin V function in organelle trafficking. Biol Cell 99, 411–423.

Evans RD, Robinson C, Briggs DA, Tooth DJ, Ramalho JS, Cantero M, Montoliu L, Patel S, Sviderskaya EV, Hume AN (2014). Myosin-Va and dynamic actin oppose microtubules to drive long-range organelle transport. Curr Biol 24, 1743–1750.

Flory PJ (1953). Principles of polymer chemistry, New York: Cornell University Press.

Forkey JN, Quinlan ME, Shaw MA, Corrie JET, Goldman YE (2003). Three-dimensional structural dynamics of myosin V by single-molecular fluorescence polarization. Nature 422, 399–404.

Goff LL, Amblard F, Furst EM (2001). Motor-driven dynamics in actin-myosin networks. Phys Rev Lett 88, 018101.

Gross SP, Tuma MC, Deacon SW, Serpinskaya AS, Reilein AR, Gelfand VI (2002). Interactions and regulation of molecular motors in Xenopus melanophores. J Cell Biol 156, 855–865.

Hammer III, JA, Sellers JR (2012). Walking to work: roles for class V myosins as cargo transporters. Nat Rev Mol Cell Biol 13, 13–26.

Heaslip AT, Nelson SR, Lombardo AT, Previs SB, Armstrong J, Warshaw DM (2014). Cytoskeletal dependence of insulin granule movement dynamics in INS-1 beta-cells in response to glucose. PLoS One 9, e109082.

Humphrey D, Duggan C, Saha D, Smith D, Käs J (2002). Active fluidization of polymer networks through molecular motors. Nature 416, 413–416.

Jung W, Tabatabai AP, Thomas JJ, Tabei SMA, Murrell MP, Kim T (2019). Dynamic motions of molecular motors in the actin cytoskeleton. Cytoskeleton 76, 517–531.

Koenderink GH, Dogic Z, Nakamura F, Bendix PM, MacKintosh FC, Hartwig JH, Stossel TP, Weitz DA (2009). An active biopolymer network controlled by molecular motors, Proc Natl Acad Sci USA 106, 15192–15197.

Lan G, Sun SX (2005). Dynamics of myosin-V processivity. Biophys J 88, 999–1008.

Liverpool TB, Maggs AC, Ajdari A (2001). Viscoelasticity of solutions of motile polymers. Phys Rev Lett 86, 4171.

Lombardo AT, Nelson SR, Ali MY, Kennedy GG, Trybus KM, Walcott S, Warshaw DM (2017). Myosin Va molecular motors manoeuvre liposome cargo through suspended actin filament intersection *in vitro*. Nat Commun 8, 15692.

Lombardo AT, Nelson SR, Kennedy GG, Trybus KM, Walcott S, Warshaw DM (2019). Myosin Va transport of liposomes in three-dimensional actin networks is modulated by actin filament density, position and polarity. Proc Natl Acad Sci USA 116, 8326–8335.

Mizuno D, Tardin C, Schmidt CF, MacKintosh FC (2007). Nonequilibrium mechanics of active cytoskeletal networks. Science 315, 370–373.

Murrell MP, Gardel ML (2012). F-actin buckling coordinates contractility and severing in a biomimetic actomyosin cortex model. Proc Natl Acad Sci USA 109, 20820–20825.

Nelson SR, Trybus KM, Warshaw DM (2014). Motor coupling through lipid membranes enhances transport velocities for ensembles of myosin Va. Proc Natl Acad Sci USA 111, 3986–3995.

Newman MEJ, Watts DJ (1999). Scaling and percolation in the small-world network model. Phys Rev E 60, 7332.
Pastural E, Barrat FJ, Dufourcq-Lagelouse R, Certain S, Sanal O, Jabado N, Seger R, Griscelli C, Fischer A, de Saint Basile G (1997). Griscelli disease maps to chromosome 15q21 and is associated with mutations in the myosin-Va gene, Nat Genet 16, 289–292.
Porat-Shliom N, Milberg O, Masedunskas A, Weigert R (2013). Multiple roles for the actin cytoskeleton during regulated exocytosis. Cell Mol Life Sci 70, 2099–2121.
Provance Jr., DW, Wei M, Ipe V, Mercer JA (1996). Cultured melanocytes from dilute mutant mice exhibit dendritic morphology and altered melanosome distribution, Proc Natl Acad Sci USA 93, 14554–14558.
Rorsman P, Renström (2003). Insulin granule dynamics in pancreatic beta cells. Diabetologia 46, 1029–1045.
Ross JL, Ali MY, Warshaw DM (2008). Cargo transport: molecular motors navigate a complex cytoskeleton. Curr Opin Cell Biol 20, 41–47.
Scholz M, Burov S, Weirich KL, Scholz BJ, Tabei SMA, Gardel ML, Dinner AR (2016). Cycling state that can lead to glassy dynamics in intracellular transport. Phys Rev X 6, 011037.
Scholz M, Weirich KL, Gardel ML, Dinner AR (2020). Tuning molecular motor transport through cytoskeletal filament network organization. Soft Matter 16, 2135–2140.
Schuh M (2011). An actin-dependent mechanism for long-range vesicle transport. Nat Cell Biol 13, 1431–1436.
Sheinman M, Broedersz CP, MacKintosh FC (2012a). Nonlinear effective-medium theory of disordered spring networks. Phys Rev E 85, 021801.
Sheinman M, Broedersz CP, MacKintosh FC (2012b). Actively stressed marginal networks. Phys Rev Lett 109, 238101.
Soares e Silva M, Depken M, Stuhrmann B, Korsten M, MacKintosh FC,Koenderink, GH (2011). Active multistage coarsening of actin networks driven by myosin motors, Proc Natl Acad Sci USA 108, 9408–9413.
Solé RV, Rosas-Casals M, Corominas-Murtra B, Valverdi S (2008). Robustness of the European power grids under intentional attack. Phys Rev E 77, 026102.
Stauffer D (1976). Gelation in concentrated critically branched polymer solutions. Percolation scaling theory of intramolecular bond cycles. J Chem Soc Faraday Trans 272, 1354–1364.
Stockmayer WH (1943). Theory of molecular size distribution and gel formation in branched-chain polymers. J Chem Phys 11, 45.
Tabb JS, Molyneaux BJ, Cohen DL, Kuznetsov SA, Langford GM (1998). Transport of ER vesicles on actin filaments in neurons by myosin V. J Cell Sci 111, 3221–3234.
Takagishi Y, Murata Y (2006). Myosin Va mutation in rats is an animal model for the human hereditary neurological disease, Griscelli syndrome type 1. Ann NY Acad Sci 1086, 66–80.
Veigel C, Wang F, Bartoo ML, Sellers JR, Molloy JE (2002). The gated gait of the processive molecular motor, myosin V. Nat Cell Biol 4, 59–65.
Vilfan A (2005). Elastic level-arm model for myosin V. Biophys J 88, 3792–3805.
Wagner W, Brenowitz SD, Hammer, JA III (2011). Myosin-Va transports the endoplasmic reticulum into the dendritic spines of Purkinje neurons. Nat Cell Biol 13, 40–48.
Warshaw DM, Kennedy GG, Work SS, Krementsova EB, Beck S, Trybus KM (2005). Differential labeling of myosin V heads with quantum dots allows direct visualization of hand-over-hand processivity. Biophys J 88, L30–L32.
Yildiz A, Forkey JN, McKinney SA, Ha T, Goldman YE, Selvin PR (2003). Myosin V walks hand-over-hand: single fluorophore imaging with 1.5-nm localization. Science 300, 2061–2065.